Available online at www.sciencedirect.com
SCIENCE DIRECT®
Journal of Solid State Chemistry 177 (2004) 4695–4700
JOURNAL OF SOLID STATE CHEMISTRY
www.elsevier.com/locate/jssc

# Synthesis, structure, and physical properties of $Ce_2PdGa_{10}$

Jasmine N. Millican[a], Robin T. Macaluso[a], D.P. Young[b], M. Moldovan[b], Julia Y. Chan[a,*]

[a] Department of Chemistry, Louisiana State University, Room 232, Choppin Hall, Baton Rouge, LA 70803, USA
[b] Department of Physics and Astronomy, Louisiana State University, Baton Rouge, LA 70803, USA

Received 2 July 2004; received in revised form 16 August 2004; accepted 21 August 2004

**Abstract**

A new ternary compound, $Ce_2PdGa_{10}$, has been synthesized using Ga flux and characterized by single-crystal X-ray diffraction. $Ce_2PdGa_{10}$ adopts a tetragonal structure in the $I_4/mmm$ space group and is isostructural to $Ce_2NiGa_{10}$. Lattice parameters are $a = 4.3230(3)$ Å, $c = 26.536(3)$ Å, $V = 495.91(7)$ Å$^3$, and $Z = 2$. The compound is metallic ($d\rho/dT > 0$), with the resistance decreasing roughly linearly with temperature from 300 to 175 K. The magnetic susceptibility of $Ce_2PdGa_{10}$ is consistent with local-moment paramagnetism and no long-range magnetic ordering occurs down to 2 K. A large positive magnetoresistance over 200% is observed at 2 K for fields of 9 T. In this paper, we present the structure and physical properties of $Ce_2PdGa_{10}$ and compared them to $CePdGa_6$.


*Keywords:* $Ce_2PdGa_{10}$; $CePdGa_6$; Flux growth; Single-crystal X-ray diffraction; Magnetic susceptibility; Magnetoresistance; Gallides; Rare-earth element intermetallics

## 1. Introduction

Heavy fermion compounds are of particular interest because of the interplay between the local magnetic moment and conduction electrons which yields large effective masses, long-range magnetic order, and in rare cases even superconductivity [1,2]. Several ternary Ce–*M*–*X* (*M* = transition metal, *X* = main group element) compounds are of notable interest due to their interesting structural and physical properties. It has been recently shown that $Ce_nMIn_{3n+2}$ ($n = 1, 2, \infty$; *M* = Co, Rh, or Ir) [1,2] are heavy fermion compounds, where $CeCoIn_5$ exhibits the highest superconducting transition temperature ($T_C = 2.3$ K) of any Ce-based heavy fermion material [1]. Although the origin of superconductivity in heavy fermion materials remains an unresolved issue, there is growing evidence that the superconductivity found in $CeCoIn_5$ may be magnetically mediated [1]. $Ce_nRhIn_{3n+2}$ ($n = 1, 2$) and $CeIn_3$ ($n = \infty$) compounds comprise a homologous series that display both antiferromagnetic and superconducting behavior [3–5]. The fact that both antiferromagnetism and superconductivity occur in the $Ce_nRhIn_{3n+2}$ ($n = 1, 2$) and $CeIn_3$ ($n = \infty$) compounds has been correlated with minimal distortions in the $CeIn_3$ cuboctahedra layer. Although distortions have been found for the *M* = Co or Ir in the $Ce_nMIn_{3n+2}$ analogues [6], they exhibit superconductivity at ambient pressure [1,2].

Recently, $CePdGa_6$ was found to be a heavy fermion compound with $\gamma \sim 300$ mJ/mol K$^2$ [7]. $CePdGa_6$ exhibits an antiferromagnetic transition along its *c*-axis at $T_N = 5.5$ K. Its structure consists of a periodic stacking of $CeGa_{8/4}$ layers and $PdGa_{8/2}$ layers along the *c*-axis. In our exploration of structurally related Ce compounds, we have synthesized a new ternary phase, $Ce_2PdGa_{10}$. The structure and physical properties of $Ce_2PdGa_{10}$ will be presented and compared with $CePdGa_6$ to determine how structural features may affect magnetic properties in these compounds.

*Corresponding author. Fax: +1-225-578-3458.
*E-mail address:* jchan@lsu.edu (J.Y. Chan).

0022-4596/$ - see front matter © 2004 Elsevier Inc. All rights reserved.
doi:10.1016/j.jssc.2004.08.030

## 2. Experimental

### 2.1. Synthesis

Single crystals of $Ce_2PdGa_{10}$ were synthesized by flux growth. In synthesizing a wide range of different ternary inter-metallic compounds by flux growth, the starting stoichiometric ratios are often quite similar. Interestingly, $Ce_2PdGa_{10}$ has the same starting stoichiometric ratio and a similar heat treatment as $CePdGa_6$ [7]. However, the cooling rates and final dwell temperatures are varied, and the final dwell temperature, independent of the starting stoichiometric ratio, may be key in determining which phase will be thermodynamically favored.

The starting materials, Ce ingot (3N, Ames Laboratory), Pd powder (5N, Alfa Aesar), and Ga shot (5N, Alfa Aesar), were placed in a 5-mL alumina crucible in a 1:1:20 ratio. The sample was sealed in an evacuated silica tube and heated at 1423 K for 7 h. Upon slow cooling to a final dwell temperature of 773 K at a rate of 281 K/h, the sample tube was then inverted and centrifuged for 5 min to remove excess Ga flux. Silver-color plate-shaped crystals were found, and typical crystal size ranged from $1\times2\times2$ to $1\times5\times5\,mm^3$. The crystalline samples were not observed to decompose in air.

### 2.2. Single-crystal X-ray diffraction

A fragment of a single crystal of size $0.025\times0.05\times0.05\,mm^3$ was mounted onto the goniometer of a Nonius KappaCCD diffractometer equipped with a Mo$K\alpha$ radiation ($\lambda=0.71073$ Å) X-ray tube. Data were collected, and the structural model was refined using SHELXL97 [8]. The atomic positions from the $Ce_2NiGa_{10}$ structure type [9] were used as an initial structural model in determining the atomic positions for $Ce_2PdGa_{10}$. Crystallographic parameters are presented in Table 1. Corrections were made for extinction, and the data were refined with anisotropic displacement parameters. Atomic positions and related structural information are provided in Table 2. Selected inter-atomic bond distances and bond angles are given in Table 3. To ensure sample homogeneity, three separate batches of $Ce_2PdGa_{10}$ crystals were characterized by single-crystal X-ray diffraction.

### 2.3. Physical property measurements

The electrical resistivity and magnetoresistance (MR) of a single crystal of $Ce_2PdGa_{10}$ were measured by the standard four-probe AC technique at 27 Hz. Pt wires (0.002 in diameter) were attached to the sample with Epotech silver epoxy. The sample was vapor cooled in a Quantum Design cryostat. The bulk magnetic susceptibility and magnetization versus field were also measured in a PPMS system from Quantum Design in fields up to 9 T.

Table 1
Crystallographic parameters

| | |
|---|---|
| *Crystal data* | |
| Formula | $Ce_2PdGa_{10}$ |
| $a$ (Å) | 4.3230(3) |
| $c$ (Å) | 26.536(3) |
| $V$ (Å$^3$) | 495.91(7) |
| $Z$ | 2 |
| Crystal dimension (mm$^3$) | $0.05\times0.025\times0.005$ |
| Crystal system | Tetragonal |
| Space group | $I_4/mmm$ |
| $\theta$ range (deg.) | 2.55–32.03 |
| $\mu$ (1/mm) | 59.47 |
| *Data collection* | |
| Measured reflections | 1182 |
| Independent reflections | 296 |
| Reflections with $I>2\sigma(I)$ | 198 |
| $R_{int}$ | 0.025 |
| $h$ | $-5\rightarrow5$ |
| $k$ | $-3\rightarrow3$ |
| $l$ | $-28\rightarrow34$ |
| *Refinement* | |
| [a] $R[F^2>2\sigma(F^2)]$ | 0.0271 |
| [b] w$R(F^2)$ | 0.0629 |
| Reflections | 214 |
| Parameters | 19 |
| $\Delta\rho_{max}$ (e/Å$^3$) | 1.350 |
| $\Delta\rho_{min}$ (e/Å$^3$) | −1.370 |
| Extinction coefficient | 0.001(17) |

[a] $R_1=\sum||F_o|-|F_c||/\sum|F_o|$.
[b] $wR_2=\left[\sum[w(F_o^2-F_c^2)]/\sum[w(F_o^2)^2]\right]^{1/2}$.

Table 2
Atomic positions and displacement parameters in $Ce_2PdGa_{10}$

| Atom | Wyckoff position | $x$ | $y$ | $z$ | $U_{eq}$ [a] |
|---|---|---|---|---|---|
| Ce | 4*e* | 0 | 0 | 0.35289(3) | 0.01083(34) |
| Pd | 2*b* | 0 | 0 | $\frac{1}{2}$ | 0.00972(44) |
| Ga1 | 4*d* | 0 | $\frac{1}{2}$ | $\frac{1}{4}$ | 0.01249(47) |
| Ga2 | 8*g* | $\frac{1}{2}$ | 0 | 0.448564(4) | 0.01143(39) |
| Ga3 | 4*e* | 0 | 0 | 0.106093(7) | 0.01657(49) |
| Ga4 | 4*e* | 0 | 0 | 0.197678(6) | 0.01152(46) |

[a] $U_{eq}$ is defined as one-third of the trace of the orthogonalized $U_{ij}$ tensor.

## 3. Results and discussion

### 3.1. Structure

Fig. 1 shows the crystal structures of $CePdGa_6$ and $Ce_2PdGa_{10}$ for comparison. $Ce_2PdGa_{10}$ crystallizes in

Table 3
Selected inter-atomic distances (Å) and bond angles (deg.) of $Ce_2PdGa_{10}$

| | |
|---|---|
| *Ce–Ga3 layer* | |
| Ce–Ga3 ( × 4) | 3.2448(7) (Å) |
| Angles (°) | |
| Ga3–Ce–Ga3 | 83.54(2) |
| *$PdGa_{8/4}$ rectangular prism* | |
| $PdGa_{8/4}$ ( × 8) | 2.5564(6) (Å) |
| Angles (°) | |
| Ga2–Pd–Ga2 | 73.44(2) |
| | 115.46(4) |
| | 64.54(4) |
| *Ga1–Ga4 tetrahedral slab layers* | |
| Ga1–Ga4 ( × 4) | 2.5690(9) (Å) |
| Ga4–Ga3 ( × 1) | 2.430(3) (Å) |
| Angles (°) | |
| Ga1–Ga4–Ga1 | 73.02(3) |
| Ga4–Ga1–Ga4 | 106.98(3) |
| | 114.57(6) |

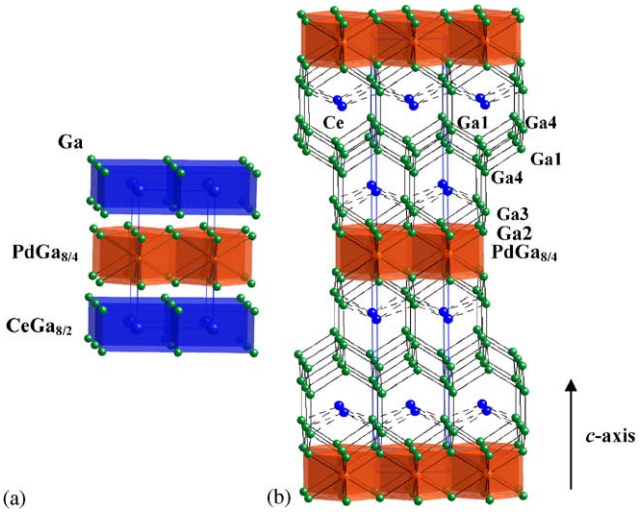


Fig. 1. Crystal structures of (a) $CePdGa_6$ and (b) $Ce_2PdGa_{10}$ are shown along the *c*-axis. (a) Face-sharing eight-coordinate Ce rectangular prisms are blue; edge-sharing Pd rectangular prisms are orange; and Ga atoms are green circles. (b) Ce atoms of the Ce–Ga3 layers are blue; edge-sharing Pd rectangular prisms are orange; and Ga atoms are denoted as green circles.

the tetragonal $I_4/mmm$ space group (No. 139) with the Ce, Pd, Ga1, Ga2, Ga3, and Ga4 atoms occupying the 4*e*, 2*b*, 4*d*, 8*g*, 4*e*, and 4*e* Wyckoff symmetry sites, respectively. $Ce_2PdGa_{10}$ has lattice parameters of $a = 4.3230(3)$ Å, $c = 26.536(3)$ Å, and $Z = 2$.

$Ce_2PdGa_{10}$ is isostructural to $Ce_2NiGa_{10}$ [9] and $Ce_2NiAl_{6-x}Ge_{4-y}$ [10]. Both compounds have similar lattice parameters (~4 × 26 Å) and cell volumes of approximately 500 $Å^3$. The overall structure of $Ce_2M Ga_{10}$ ($M$ = Ni or Pd) can be viewed as a periodic stacking of alternating staggered rare-earth bilayers and Ga3/Ga2/$M$/Ga2/Ga3 layers, forming a "sandwich" structure along the *c*-axis. Ga1–Ga4 tetrahedral slabs separate each Ce bilayer along the *c*-axis.

At a glance, the crystal structure of $Ce_2PdGa_{10}$ closely resembles that of $CePdGa_6$ [7]. The structure of $CePdGa_6$ can be viewed as layers of face-sharing eight-coordinate $CeGa_{8/4}$ rectangular prisms, alternating with layers of $PdGa_{8/2}$ rectangular prisms along the *c*-axis. However, in $Ce_2PdGa_{10}$, the Ga2 atoms of the edge-sharing $PdGa_{8/2}$ rectangular prisms are capped by Ga3 atoms above and below to form Ga3/Ga2/Pd/Ga2/Ga3 slabs. These Ga3/Ga2/Pd/Ga2/Ga3 slabs are between staggered bilayers of Ce atoms along the *c*-axis. With a bonding cutoff of 3.25 Å, these Ce atoms are coordinated to four Ga3 atoms with an inter-atomic distance of 3.2448(7) Å. However, the Ce···Ga1 and Ce···Ga4 inter-atomic distances of 3.4823(7) Å and 3.3384(8) Å, respectively, are too long to be considered bonding when compared to the expected inter-atomic distance of 3.17 Å, projected by the sum of the Ce (1.82 Å) and Ga (1.35 Å) covalent radii [11]. Thus, the Ce···Ga1 and Ce···Ga4 may represent weak bonding interactions. The Ga3···Ga3 inter-atomic distance of 4.323(1) Å found within these Ce layers is also too long to be considered bonding when compared to the sum of covalent radii of Ga (1.35 Å) [11]. However, the Ce–Ga3 inter-atomic distances are 3.2448(7) Å and within the 3.111–3.299 Å range found in the binary compounds $CeGa_6$ [12], $CeGa_2$ [13], and $Ce_5Ga_3$ [13]. These distances are slightly larger than the expected Ce–Ga inter-atomic distance of 3.17 Å, projected by the sum of the Ce (1.82 Å) and Ga (1.35 Å) covalent radii [11].

Pd atoms are located at the center of the rectangular prisms and are coordinated to Ga2 atoms at the vertices. The Pd–Ga2 inter-atomic distance is 2.5564(6) Å, which is consistent with other known Pd–Ga inter-atomic distances. In $Pd_2Ga$ and $CePdGa_6$, for example, the Pd and Ga atoms are separated by 2.558 Å [14] and 2.5609(4) Å [7], respectively. The Pd–Ga2 inter-atomic distances of 2.5564(6) Å in $Ce_2PdGa_{10}$ are also within the expected inter-atomic distance of 2.72 Å based on the summation of the covalent radii of Pd (1.37 Å) and Ga (1.35 Å) [11]. In the $PdGa_{8/4}$ rectangular prisms of $Ce_2PdGa_{10}$, the Ga2–Ga2 distance along the *c*-axis is 2.730(2) Å, which is consistent with the expected Ga–Ga inter-atomic distance of 2.70 Å, the sum of the covalent radii of Ga (1.35 Å) [11] and consistent with the Ga–Ga bond of 2.7039(15) and 2.46(2)–2.792(11) Å in $CePdGa_6$ and elemental Ga, respectively [15].

In contrast to $CePdGa_6$, however, each Ce bilayer in $Ce_2PdGa_{10}$ is separated by Ga1–Ga4 tetrahedral slabs along the *c*-axis, where each Ga atom is in a tetrahedral environment. The Ga1–Ga4 inter-atomic distance of 2.569(9) Å within these slabs is consistent with the expected Ga–Ga inter-atomic distance of

2.70 Å [11]. Ga4–Ga1–Ga4 bond angles in the Ga1–Ga4 tetrahedron are 106.98(3)° and 114.57(6)°, respectively, which are slightly distorted. Each layer of the Ga1–Ga4 tetrahedra is linked to the Ga3 atom of the adjacent Ce–Ga3 layer by a Ga4–Ga3 inter-atomic distance of 2.430(3) Å along the *c*-axis. This linkage forms a cage-like structure, where each "cage" encapsulates one Ce atom, similar to the structure of the $ThCr_2Si_2$ type [16].

### 3.2. Physical properties

Fig. 2 shows the electrical resistivity as a function of temperature for a single crystal of $Ce_2PdGa_{10}$. The data are shown for current being applied in the *ab*-plane. The sample is metallic ($d\rho/dT>0$), with the resistance decreasing roughly linearly with temperature from 300 to 175 K. Below 50 K the slope of the resistivity begins to increase, and the value of the resistivity drops by a factor of 4 at low temperature. This behavior is typical of Kondo compounds, where the drop in the resistivity indicates the onset of Kondo coherence. The electrical resistivity of single crystals of $CePdGa_6$ in the *ab*-plane also has a similar behavior [17]. We attempted to measure the resistivity with current applied along the *c*-axis; however, the samples were too small to do this accurately in conjunction with the usual difficulties in performing a four-probe measurement on a thin flat sample perpendicular to the plane.

Fig. 3 shows the in-plane MR ($MR(\%)=[(\rho(H)-\rho(0))/\rho(0)]\times 100$) of a single crystal of $Ce_2PdGa_{10}$ as a function of field at 2 K [18]. The MR is positive and large at 2 K, increasing by over 200% at 9 T, which is quite unusual for most inter-metallic compounds at low temperatures. Other inter-metallics that exhibit positive MR are on the order of MR% < 120% up to fields of 9 T [18–20]. For example, $SmPd_2Ga_2$ has a positive MR at 2 K, but the MR% < 120% at 9 T [19]. Although the magnitude of the MR for $Ce_2PdGa_{10}$ is unusual, a classical effect is observed as the MR saturates up to fields of 9 T. The MR tends to follow the curve of a paramagnet induced with field as suggested by the magnetization data in Fig. 5. The large MR may be attributed to increasing spin disorder scattering which is not uncommon in the paramagnetic systems, where electrons are scattered on entirely disordered magnetic moments [21].

In the main panel of Fig. 4, the magnetic susceptibility of a single crystal of $Ce_2PdGa_{10}$ is shown as a function of temperature for the field perpendicular to the *ab*-plane. The sample was zero field cooled (ZFC) and then warmed in a constant field of 0.1 T. The data are well fit by the solid line in the main panel of Fig. 4, which represents a modified Curie law of the form $\chi=M/H=\chi_o+C/T$, where $\chi_o$ is the some temperature-independent background susceptibility. From the fit, $\chi_o=7.67\times10^{-4}\,\mu_B$/mol, and the Curie constant, *C*, has a value of $1.39\times10^{-4}\,\mu_B$ K/mol. This results in an effective magnetic moment of 2.5 $\mu_B$/mol Ce. This value is consistent with what one would expect for the full Hund's rule moment of 2.54 $\mu_B$ for Ce in its 3+ state. The magnetic susceptibility of $Ce_2PdGa_{10}$ is consistent with local-moment paramagnetism, and no long-range magnetic order occurs down to 2 K. The inset of Fig. 4 shows inverse susceptibility ($1/\chi$) as a function of field at 2 K. The data follow Curie–Weiss behavior from 0 to 170 K.

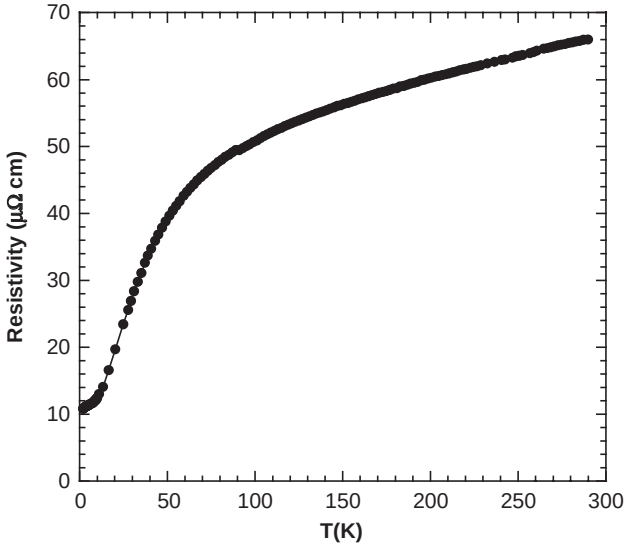


Fig. 2. Normalized electrical resistivity of a single crystal of $Ce_2PdGa_{10}$ as a function of temperature. The data are taken for the current parallel to the *ab*-plane.

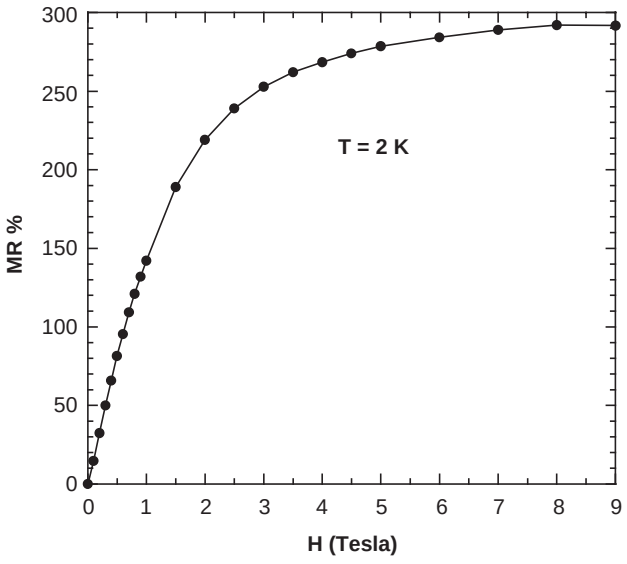


Fig. 3. MR of a single crystal of $Ce_2PdGa_{10}$ as a function of field at 2 K. The data are taken for the field parallel to the *ab*-plane.

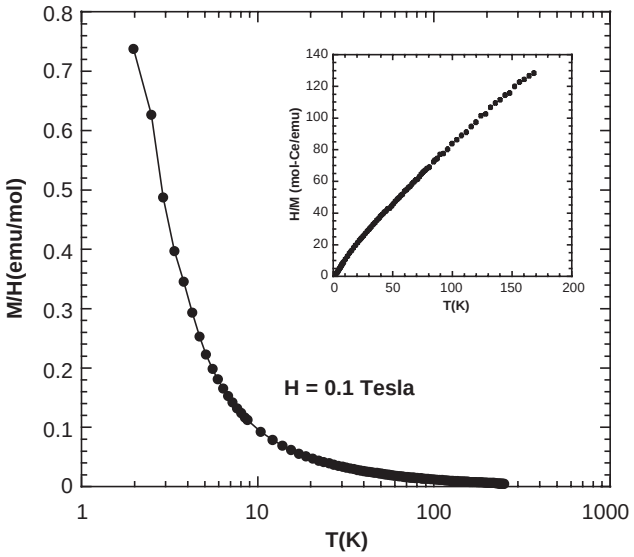


Fig. 4. Magnetic susceptibility of a single crystal of $Ce_2PdGa_{10}$ as a function of temperature for field perpendicular to the *ab*-plane. The sample was ZFC and then warmed in a constant field of 0.1 T. The inset shows inverse susceptibility with Curie–Weiss behavior as a function of temperature from 0 to 170 K. The solid lines in the figures are a fit to the data as described in the text.

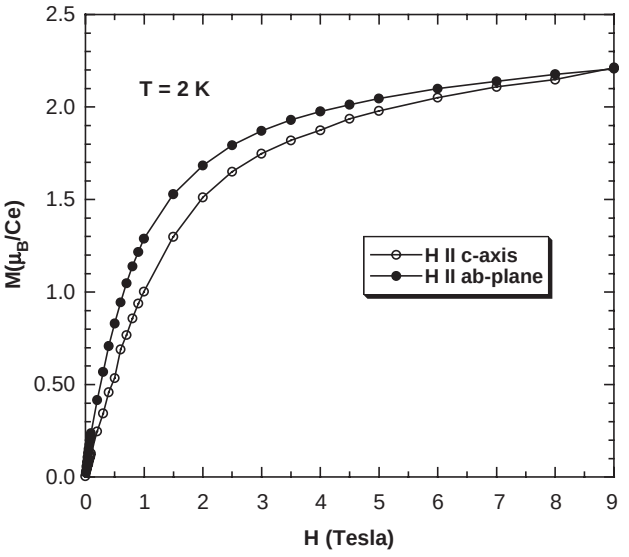


Fig. 5. Magnetization versus field for a single crystal of $Ce_2PdGa_{10}$ at 2 K. Closed and open circles represent data for the field parallel to the *ab*-plane and *c*-axis, respectively.

Plotted in Fig. 5 is the magnetization of a single crystal of $Ce_2PdGa_{10}$ at 2 K as a function of applied magnetic field. The open circles represent data for the field applied perpendicular to the *ab*-plane, and the solid circles are for the field parallel to the *ab*-plane. There is a small amount of magnetic anisotropy between the two field orientations at low field, with the magnetization being slightly larger for the parallel field, and essentially no anisotropy at higher fields. The data are again consistent with local-moment paramagnetism, and no hysteresis was observed in any field orientation. The magnetization in both field directions has not saturated even to 9 T.

## 4. Conclusion

Because $Ce_2PdGa_{10}$ has similar structural units as $CePdGa_6$, a correlation may exist between anomalies in their structures and physical properties. Previous work has shown that the antiferromagnetic behavior of $CePdGa_6$ can be attributed to competition between the Kondo effect and RKKY-like mechanisms [7]. The lack of magnetic ordering in $Ce_2PdGa_{10}$ may be due to the reduced Ce–Ce interactions due to the Ga1–Ga4 tetrahedral slab layers in the structure. Fewer Ce–Ga contacts are found in $Ce_2PdGa_{10}$; Ce is coordinated to only four Ga atoms, whereas Ce is coordinated to eight Ga atoms in $CePdGa_6$. This reduced hybridization may be responsible for reduced RKKY interactions, and consequently, paramagnetic behavior. In addition, these Ga1–Ga4 tetrahedral slab layers separate the Ce layers, possibly inhibiting the magnetic exchange in RKKY-like interactions even further. As a result, the Ce moments may become more localized, and the Kondo effect to be more pronounced than RKKY interactions. Evidence of the Kondo coherence is observed in resistivity data. Further calculations of the band structure will provide more insight into the Ce interactions.

## Acknowledgments

J.Y.C. acknowledges the Louisiana Board of Regents, PRF-G, and NSF Career (DMR 0237664) and Alfred P. Sloan Fellowship for partial support of this project.

## References

[1] C. Petrovic, P.G. Pagliuso, M.F. Hundley, R. Movschovich, J.L. Sarrao, J.D. Thompson, Z. Fisk, P. Monthoux, J. Phys.: Condens. Matter 13 (2001) L337.
[2] C. Petrovic, R. Movshovich, M. Jaime, P.G. Pagliuso, M.F. Hundley, J.L. Sarrao, Z. Fisk, J.D. Thompson, Europhys. Lett. 53 (2001) 354.
[3] H. Hegger, E.G. Moshopoulou, M.F. Hundley, J.L. Sarrao, Z. Fisk, J.D. Thompson, Phys. Rev. Lett. 84 (2000) 4986.
[4] A.L. Cornelius, A.J. Arko, J.L. Sarrao, M.F. Hundley, Z. Fisk, Phys. Rev. B 62 (2000) 14 182.
[5] J.D. Thompson, R. Movshovich, Z. Fisk, F. Bouquet, N.J. Curro, R.A. Fisher, P.C. Hammel, H. Hegger, M.F. Hundley, M. Jaime,

P.G. Pagliuso, C. Petrovic, N.E. Phillips, J.L. Sarrao, J. Magn. Magn. Mater. 226 (2001) 5.
[6] R.T. Macaluso, J.L. Sarrao, N.O. Moreno, P.G. Pagliuso, J.D. Thompson, F.R. Froncek, M.F. Hundley, A. Malinowski, J.Y. Chan, Chem. Mater. 15 (2003) 1394.
[7] R.T. Macaluso, S. Nakatsuji, H. Lee, Z. Fisk, M. Moldovan, D.P. Young, J.Y. Chan, J. Solid State Chem. 174 (2003) 296.
[8] G.M. Sheldrick, SHELXL97, University of Göttingen, Germany, 1997.
[9] Y. Yarmolyuk, Y. Grin, I. Rozhdestvenskaya, O. Usov, A. Kuz'min, V. Bruskov, E. Gladyshevskii, Sov. Phys. Crystallogr. 27 (1982) 599.
[10] B. Sieve, P. Trikalitis, M. Kanatzidis, Z. Anorg. Allg. Chem. 628 (2002) 1568.
[11] U. Müller, Inorganic Structural Chemistry, Wiley, New York, 1993, p. 32.
[12] J. Pelleg, G. Kimmel, D. Dayan, J. Less-Common Met. 81 (1981) 33.
[13] G. Kimmel, D. Dayan, A. Grill, J. Pelleg, J. Less-Common Met. 75 (1980) 133.
[14] R. Welter, G. Venturini, B. Malaman, J. Less-Common Met. 329 (2001) 69.
[15] J. Donohue, The Structures of the Elements, Wiley, New York, 1974.
[16] C. Zheng, R. Hoffmann, J. Solid State Chem. 72 (1988) 58.
[17] M. Moldovan, L.L.H.R.G. Goodrich, R.T. Macaluso, J.Y. Chan, P.W. Adams, D.P. Young, 2004, in preparation.
[18] L. Deakin, A. Mar, Chem. Mater. 15 (2003) 3343.
[19] W.M. Williams, R.T. Macaluso, M. Moldovan, D.P. Young, J.Y. Chan, Inorg. Chem. 42 (2003) 7315.
[20] W.R. Branford, S.K. Clowes, M.H. Syed, Y.V. Bugoslavsky, C.E.A. Grigorescu, A.V. Berenov, S.B. Roy, L.F. Cohen, Appl. Phys. Lett. 84 (2004) 2358.
[21] V. Sechovský, L. Havela, K. Prokeš, H. Nakotte, F.R. de Boer, E. Brück, J. Appl. Phys. 76 (1994) 6913.